PAPER

On the ground state of one-dimensional quantum droplets for large chemical potentials

IOP Publishing Journal of Physics A: Mathematical and Theoretical
J. Phys. A: Math. Theor. **57** (2024) 445701 (12pp) https://doi.org/10.1088/1751-8121/ad82bb

On the ground state of one-dimensional quantum droplets for large chemical potentials

J Holmer[1], K Z Zhang[2] and P G Kevrekidis[3,*]

[1] Department of Mathematics, Brown University, Providence, RI 02912, United States of America
[2] Department of Mathematics, Northeastern University, Boston, MA 02115, United States of America
[3] Department of Mathematics and Statistics, University of Massachusetts, Amherst, MA 01003-4515, United States of America

E-mail: kevrekid@umass.edu

Received 27 April 2024; revised 27 August 2024
Accepted for publication 1 October 2024
Published 14 October 2024

Abstract

In the present work we revisit the problem of the quantum droplet in atomic Bose–Einstein condensates with an eye towards describing its ground state in the large density, so-called Thomas–Fermi (TF) limit. We consider the problem as being separable into 3 distinct regions: an inner one, where the TF approximation is valid, a sharp transition region where the density abruptly drops towards the (vanishing) background value and an outer region which asymptotes to the background value. We analyze the spatial extent of each of these regions, and develop a systematic effective description of the rapid intermediate transition region. Accordingly, we derive a uniformly valid description of the ground state that is found to accurately match our numerical computations. As an additional application of our considerations, we show that this formulation allows for an analytical approximation of excited states such as the (trapped) dark soliton in the large density limit.

Keywords: quantum droplets, Thomas–Fermi limit, ground state, extended gross-pitaevskii equation, dark solitons

1. Introduction

Over the past few years, an emerging topic in the physics of atomic Bose–Einstein condensates has been the exploration of quantum droplets. The latter constitute self-bound states arising

* Author to whom any correspondence should be addressed.

from the interplay between the mean-field and quantum fluctuation energetic contributions [1]. In this competition, it is also important to recognize the role of the system's dimensionality [2]. Early experimental observations of the relevant settings took place in dipolar condensates [3, 4], followed shortly thereafter by trapped bosonic mixtures with contact interactions [5–7]. Such droplet states were also observed in free space, e.g. in the work of [8].

In droplet-bearing systems, the critical role of quantum fluctuations has been theoretically incorporated by means of the well-known Lee–Huang–Yang correction term [9] that is suitably added to the standard mean-field cubic nonlinearity description [1, 10]. This leads to an extended Gross-Pitaevskii equation (EGPE) description that has been found to be fruitful for the theoretical and computational identification of such droplet patterns [11–13]. Accordingly, this formulation has been used in order to describe modulational instability and related features [14–16], collective excitations [17–20] and nonlinear wave structures in the form of solitary waves and vortices [21–27]. Indeed, already this new form of 'liquid matter' has been the subject of not only numerous studies, but also relevant reviews such as [28].

In the case of the standard single-component atomic condensates (with cubic nonlinearity), the study of the system's ground state is quite mature at this stage. For the standard one-dimensional GPE, a well-known approximation is that of the Thomas–Fermi (TF) limit, which is progressively more accurate as the chemical potential is increased and consists of an inverted parabola (with compact support) [29, 30]. What is perhaps somewhat less well-known in the physics community is that while this (TF) description is accurate close to the center of the trapped 1d condensate, there have been some significant mathematical works that have offered refinements in the vicinity of the condensate edges. In the latter, the dispersion becomes significant, creating a boundary layer which requires a more refined multiple-scales analysis to be properly captured, as has been explored in works such as those of [31, 32]. Accordingly, these works have been able to accurately approximate the relevant layer, by leveraging the so-called Hastings–McLeod solution of the Painlevé-II equation. While there exist more accurate, quasi-1d approximations of the full 3d problem [33, 34], this analysis is significant for various purposes, including towards understanding not only the asymptotics but also the excitation spectrum of the relevant ground state in an analytical (or semi-analytical/asymptotic) form.

At the present time, to the best of our knowledge, there exists no analogous analysis of the problem of the quantum droplet. In the latter case, indeed, as we will see below, the issue of the asymptotic state is further exacerbated by the attractive nature of the nonlinearity for small densities. In that light, the TF approximation fails already at a finite density and it is not possible to construct a corresponding simple-minded approximation profile by neglecting the wavefunction curvature. Accordingly, it is of interest to develop ideally a uniform approximation that allows us to capture the large chemical potential droplet wavefunction, in a way analogous to [31, 32]. This is the aim of the present work. In order to do so, we leverage a multiple-scales spatial analysis of the stationary state problem, separating the region close to the center (where the TF approximation turns out to still be valid), an intermediate, steep-descent region that we suitably quantify and finally the asymptotic decay towards the background value. Combining these 3 regions, we eventually obtain a uniform expression for the quantum droplet profile in the presence of a trap in the large chemical potential limit. This expression is of value well-beyond the strict confines of the ground state: indeed, we show that it provides us with the tools to accurately approximate excited states in the form, e.g. of the prototypical dark soliton state of the trapped system.

Our presentation will be structured as follows. In section 2 we present the mathematical setup of the problem and our main results for the droplet system's ground state. In section 3, we provide the details of our multiple-scales analysis, while in section 4 we present an extension

of the method for the case of the dark soliton configuration. Finally, in section 5, we summarize our findings and present our conclusions, as well as some directions for future work.

2. Mathematical setup & main result

The framework of interest to us herein will concern the homonuclear mass-balanced case of a one-dimensional (1d) bosonic mixture of two different (hyperfine) states. In line with earlier works including [24, 26, 27], we will assume that the two species feature equal self-repulsion $g_{11} = g_{22} \equiv g$, while across the species the attraction renders g_{12} negative. A prototypical example thereof can be encountered in the context, e.g. of ^{39}K, whose states $|1,-1\rangle$ and $|1,0\rangle$ have been considered previously [8] (in the 3d realm). Considering the relevant EGPE model

$$i u_t = -\frac{1}{2} u_{xx} + |u|^2 u - \delta |u| u + V(x)\, u. \tag{1}$$

Here, we have already assumed that the energy of the system is measured in units of $\hbar^2/(m\xi^2)$, and $\xi = \pi\hbar^2\sqrt{|\delta g|}/(mg\sqrt{2g})$ is the healing length, while the quantity $\delta g = g_{12} + g$ combines the inter- and intra-species scattering lengths. Additionally, in this formulation, time, length and wave function are scaled according to $t' = \hbar/\left(m\xi^2\right)$, $x' = \xi x$ and $u' = (2\sqrt{g})^{3/2} u/(\pi\xi\,(2|\delta g|)^{3/4})$, respectively, where the primes are used for dimensional units, and the absence thereof for dimensionless units. The potential hereafter will be assumed to have a customary parabolic profile [29, 30] of the form:

$$V(x) = \frac{1}{2}\Omega^2 x^2, \tag{2}$$

where Ω represents the effective strength of the longitudinal confinement. We note that while some of the earlier experiments have produced droplets in free space (see, e.g. [8], others such as [6] have been operating in the presence of a trap, rendering eminently relevant the considerations herein. Notice that in the case of free space, the expression for the droplet waveforms is analytically available (see, e.g. equation (7) in [17]), while this is not the case in the presence of the trap. It is our aim in the present work to provide a relevant asymptotic expression for such states in the large density, TF limit. Furthermore, we add that while considerations of losses are practically relevant to consider within an experimental setting, as with standard BECs [29, 30], it is important to firstly understand the Hamiltonian setting, and subsequently extend considerations to the presence of such losses.

As a further remark on the setting of interest, it is relevant to point out here that the scattering lengths g_{11}, g_{22} of the above hyperfine states are generically (upon variation of an external magnetic field) not equal; see, e.g. figure 1 of [8]. Nevertheless, as has been argued, e.g. in [17], in the case of smooth variations of the total density, a rescaling of the wavefunctions of the two hyperfine states still leads to the model of equation (1) and hence the model is of practical relevance to this experimentally accessible setting. The potential extension of our considerations to arbitrary density variations and values of g_{ij} is a mathematically appealing open problem that we touch upon in the outlook of the present work.

In what follows we will examine the steady state problem of equation (1) in which we will seek standing wave solutions of the form $u(x,t) = e^{-i\mu t} q(x)$, whose spatial profile will satisfy the steady state equation:

$$\mu q = -\frac{1}{2} q_{xx} + q^3 - \delta q^2 + V(x)\, q. \tag{3}$$

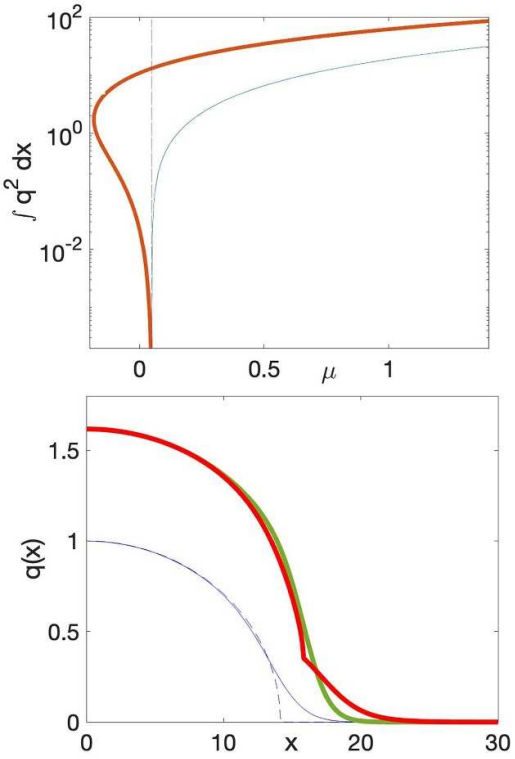

Figure 1. (Top Panel) Typical example of the ground state branch of solutions 'mass' (rescaled atom number) vs. the chemical potential μ for a parabolic trap of strength $\Omega = 0.1$ for the case of the cubic nonlinearity problem (standard GPE, thin blue line) vs. the quadratic-cubic nonlinearity of the present work (extended GPE, related to the droplet problem, red thick line). The vertical line denotes the linear (HO) limit. (Bottom panel) Prototypical example of the numerical solution (solid line) for the standard GPE (thin blue) vs. extended GPE (thick green). The analytical approximations of the TF inverted parabolic profile for the former (dashed blue) and of the present work (red) are also given for comparison. Here, the chemical potential is chosen as $\mu = 1$.

As is customary in the 1d setting [26], we will assume (without loss of generality for our standing solutions) that the spatial profile is real henceforth. Recall that the homogeneous steady states of the model are either $q = 0$ or $q = (\delta \pm \sqrt{\delta^2 + 4\mu})/2$, with the one associated with the minus sign being modulationally unstable, while the one with the plus sign being modulationally stable [14, 25].

Accordingly, the TF approximation in the presence of the trap replaces μ with $\mu - V(x)$, which can immediately be seen to be problematic when the quantity under the radical $\delta^2 + 4(\mu - V(x)) = 0$, at which point the density is finite ($q(x) = \delta/2$) and no continuous approximation leading to an asymptotically vanishing wavefunction can be constructed (contrary to the standard cubic GPE case). It is this conundrum that we wish to resolve through our analysis, providing an explicit spatial expression of increasing accuracy as μ increases for the spatially confined droplet profile. The relevant branch of solutions and the approach of its 'mass' (the scaled atom number) to the linear limit of the harmonic oscillator (HO) is shown in figure 1. The latter limit of asymptotically vanishing density pertains to the ground state of the HO with $\mu \to \Omega/2$; recall that, more generally, the linear eigenstates of the HO

have energies $\mu = (n+1/2)\Omega$, with the ground state pertaining to $n=0$. It can be seen that the cubic GPE problem monotonically tends to this limit, as is expected from its defocusing nonlinearity, while the competing nonlinearity of the quantum droplet problem is manifested in the non-monotonic approach to the relevant limit; see also [24, 26]. In the figure, we also show a prototypical example of the TF limit for $\mu = 1 \gg \Omega$. Once again, for comparison the case of the standard GPE is shown (in blue thin solid line), together with the (less refined yet straightforwardly) analytically tractable inverted parabola TF approximation (blue thin dashed line). Here, we also include for the same chemical potential the numerically exact solution of the droplet problem, obtained via a fixed point iteration, compared with our analytically derived approximate profile (both in thick lines, the former in solid green, while the latter in red). This clearly manifests the accuracy of our analytical approximation into which we now delve.

First, we proceed to change independent and dependent variables. The former change for x is intended to absorb the trap strength Ω, while the latter for q is intended to factor the nonlinearity. Changing variable

$$z = \frac{\sqrt{2}\Omega x}{\sqrt{\delta^2+4\mu}}, \qquad w = \frac{2q-\delta}{\sqrt{\delta^2+4\mu}} \tag{4}$$

gives the semiclassical form:

$$0 = -\epsilon^2 w_{zz} + \left(w^2 - f^2\right)(w+\sigma), \tag{5}$$

where $f(z)^2 = 1-z^2$ and

$$\epsilon = \frac{2\Omega}{\delta^2+4\mu}, \qquad \sigma = \frac{\delta}{\sqrt{\delta^2+4\mu}}. \tag{6}$$

The rescaling shows that despite the original form bearing three constants, there are only two actual degrees of freedom represented by ϵ and σ, and we can now focus upon the asymptotic problem of examining the behavior as $\epsilon \to 0$ for fixed σ. For $|z| \leqslant 1$, we take $f(z) = \sqrt{1-z^2}$, while outside this region $f(z) = 0$.

For fixed $0 < \sigma < 3$, we determine the form of an even solution to (5) asymptotically for $0 < \epsilon \ll 1$. The form of the nonlinearity in (5) suggests that, in regions where w is slowly oscillating, if $|z| \leqslant 1$, we should have either $w \approx f$, $w \approx -f$, or $w \approx -\sigma$. Based upon the assumption that there exists an even solution w such that $w \approx f$ for $|z| \ll 1$ and $w \to -\sigma$ as $|z| \to \infty$, we can calculate its expected functional form. The results are as follows, with the supporting calculations given in § 3.

Let $0 < z_* < 1$ be defined as the value of z at which

$$w(z_*) = \frac{f(z_*) - \sigma}{2}. \tag{7}$$

The analysis is divided into three regions (see figure 2)

- Region I, $0 \leqslant z \leqslant z_* - O(\epsilon)$, where $w \approx f$;
- Region II, $z_* - O(\epsilon) \leqslant z \leqslant z_* + O(\epsilon)$, where w rapidly transitions from $w \approx f$ to $w \approx -\sigma$;
- Region III, $z \geqslant z_* + O(\epsilon)$, where $w \approx -\sigma$.

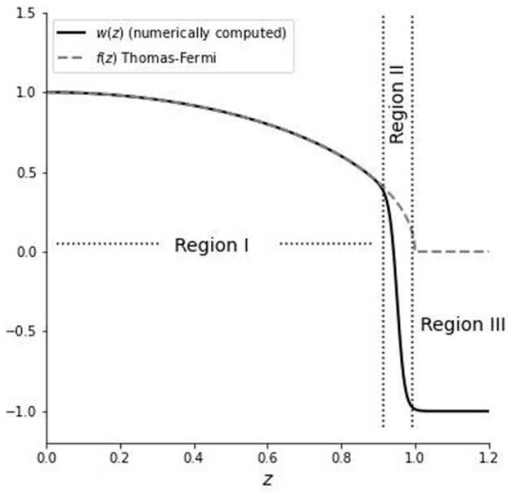

Figure 2. The different regions of analysis, shown in the case $\epsilon = 0.01$ and $\sigma = 1$. In this case, $z_* = 0.9531$ by numerical computation.

The asymptotic description of z_* and w, derived in § 3, that is uniformly valid in Regions I, II and III, is:

$$z_* = z_0 + \frac{3\sqrt{2}}{4\sigma}\epsilon + O\left(\epsilon^2\right) \tag{8}$$

where $z_0 = \sqrt{1 - \frac{\sigma^2}{9}}$ (so that $f_0 = f(z_0) = \sigma/3$) and

$$w(z) = \frac{f(z) - \sigma}{2} - \frac{f(z) + \sigma}{2} \tanh\left(\frac{2\sigma}{3\sqrt{2}} \frac{z - z_*}{\epsilon}\right). \tag{9}$$

As stated above, the result is derived for fixed $0 < \sigma < 3$ as an asymptotic expansion for $\epsilon \searrow 0$. To determine a practical range of applicability, note that Region II should be situated strictly inside $|z| \leqslant 1$. Taking z_* as given by (8), this converts to the condition

$$\epsilon < \frac{4\sigma}{3\sqrt{2}}\left(1 - \sqrt{1 - \frac{\sigma^2}{9}}\right).$$

When (8), (9) are converted using (4), (6), the result takes the form

$$x_* = \frac{1}{\sqrt{2}\Omega}\sqrt{\frac{8\delta^2}{9} + 4\mu} + \frac{1}{2} + O(\Omega) \tag{10}$$

and

$$u(x) = \frac{1}{4}\left(\delta + \sqrt{\delta^2 + 4\mu - 2\Omega^2 x^2}\right)\left(1 - \tanh\left(\frac{\delta(x - x_*)}{3}\right)\right). \tag{11}$$

In this form, the result can be interpreted as an asymptotic expansion for $\mu, \delta = O(1)$ and $0 < \Omega \ll 1$. The effective range of applicability converts to

$$\Omega < \sqrt{2}\left(\sqrt{\delta^2 + 4\mu} - \sqrt{\frac{8\delta^2}{9} + 4\mu}\right). \tag{12}$$

The upper bound (12) allows for a comparison to the case $\delta = 0$ studied by [31]. For $\mu = O(1)$, as $\delta \searrow 0$, (12) becomes $\Omega < \frac{2\delta^2}{9\sqrt{2\mu}}$, showing that Ω is pinched to zero in this limit. Indeed, x_* is approaching the boundary of the TF layer, and the refined Painlevé II asymptotics of [31] are needed for a more accurate description. It is relevant to intuitively add that the requirement of equation (12) on Ω ensures that the transition region (Region II) effectively fits within the edge of the TF region, that is to the left of the value of x at which $V(x) = \frac{1}{2}\Omega^2 x^2 = \frac{\delta^2}{4} + \mu$.

Lastly, we note that if the transition from Region II to Region III does not fit well enough inside the TF region, the slope discontinuity resulting from the TF solution will be visible. Although the overall agreement with the theory as reported is quite satisfactory, yet a discernible example of this arises in figure 1 (bottom panel). We note that here we have maintained a value of Ω that is closer to typical experimental values in terms of ratios of longitudinal to transverse one-dimensional trapping. Importantly, in the asymptotic limit $\Omega \to 0$, the transition from TF to 0 (Region II) will fit increasingly better inside the point where the TF solution reaches 0 and thus the slope discontinuity will be asymptotically invisible, rendering progressively the theory increasingly accurate.

3. Detailed analysis

To justify (8), (9), define ϕ via the equation

$$w = \frac{f-\sigma}{2} - \frac{f+\sigma}{2}\phi. \tag{13}$$

Let $y = (z - z_0)/\epsilon$. In this reference frame, Region I corresponds to $y \ll -1$, Region II lies in $-1 \lesssim y \lesssim 1$, and Region III corresponds to $y \gg 1$. Comparing (7) and (13), we see that z_* is characterized as the z-value at which $\phi(z_*) = 0$.

In Region I, $w \approx f$, so that in view of (13), we fix the $y \to -\infty$ boundary conditions as

$$\phi \to -1\,, \quad \phi_y \to 0 \quad \text{as} \quad y \to -\infty. \tag{14}$$

In Region III, $w \approx -\sigma$, so in view of (13), we set the $y \to +\infty$ boundary conditions as

$$\phi \to 1\,, \quad \phi_y \to 0 \quad \text{as} \quad y \to +\infty. \tag{15}$$

By assuming that the boundary conditions (14), (15) hold up to second order in ϵ, we will be able to obtain a consistent expansion, as follows.

Plugging (13) into (5) and changing variable $y \mapsto \xi$, with

$$\frac{\mathrm{d}\xi}{\mathrm{d}y} = \frac{f+\sigma}{2\sqrt{2}} \qquad \xi = 0 \leftrightarrow y = 0 \tag{16}$$

leads to the transformed equation

$$\phi_{\xi\xi} + 2\left(1-\phi^2\right)(\phi - h) = -\epsilon\frac{12 f_z}{\sqrt{2}\,(f+\sigma)^2}\phi_\xi + \epsilon^2\frac{8 f_{zz}}{(f+\sigma)^3}(1-\phi) \tag{17}$$

where $h = (3f-\sigma)/(f+\sigma)$. Multiplying (17) by ϕ_ξ and integrating gives

$$H(\phi,\phi_\xi)\Big]_{\xi=-\infty}^{\xi=+\infty} = \int_{-\infty}^{+\infty} R(\xi)\,\mathrm{d}\xi \tag{18}$$

where

$$\begin{aligned} H(\phi,\phi_\xi) &= \tfrac{1}{2}\phi_\xi^2 + \phi^2 - \tfrac{1}{2}\phi^4 \\ R &= 2h\left(1-\phi^2\right)\phi_\xi - \epsilon\frac{12 f_z}{\sqrt{2}\,(f+\sigma)^2}\phi_\xi^2. \end{aligned} \tag{19}$$

For the boundary values (14), (15), the left side of (18) is zero.

The equation (17) is still an exact representation of (5), but at this point we initiate an asymptotic expansion. In order that the right side of (18) vanish at zero order in ϵ, we need $h = O(\epsilon)$. Setting $h=0$ and dropping the right side of (17), it becomes $0 = \phi_{\xi\xi} + 2(1-\phi^2)\phi$, which has the solution

$$\phi(\xi) = \tanh(\xi - \xi_1)\,, \tag{20}$$

where ξ_1 is an undetermined shift. Setting $h=0$ is equivalent to setting $f = \sigma/3$. Let

$$z_0 = \sqrt{1-\frac{\sigma^2}{9}} \quad \Longleftrightarrow \quad f(z_0) = \frac{\sigma}{3}\,.$$

With z_0 as a point of reference, the asymptotic form of (16) is:

$$y = \frac{2\sqrt{2}}{f_0+\sigma}\xi + O(\epsilon)\xi^2 = \frac{3\sqrt{2}}{2\sigma}\xi + O(\epsilon)\xi^2. \tag{21}$$

The expansion of h is

$$h = -\epsilon\frac{81\sqrt{2}z_0}{8\sigma^3}\xi + O\left(\epsilon^2\right)\xi^2.$$

This and using and (20) as an approximation for ϕ in (19) provides an expansion for R:

$$R = -\epsilon\frac{81 z_0}{2\sqrt{2}\sigma^3}\left(\xi - \tfrac{1}{2}\right)\operatorname{sech}^4(\xi-\xi_1) + O\left(\epsilon^2\right).$$

Substituting this into the right side of (18) (with left side $=0$) implies that $\xi_1 = \frac{1}{2} + O(\epsilon)$ in order that the right side of (18) vanish at first order in ϵ.

Substituting (21) into $y = (z-z_0)/\epsilon$, we obtain

$$z = z_0 + \epsilon\frac{3\sqrt{2}}{2\sigma}\xi + O\left(\epsilon^2\right)\xi^2. \tag{22}$$

Recall that z_* is characterized as the z-value at which $\phi(z_*) = 0$. By (20), this corresponds to $\xi = \xi_1$ and thus

$$z_* = z_0 + \epsilon\frac{3\sqrt{2}}{2\sigma}\xi_1 + O\left(\epsilon^2\right) \tag{23}$$

which gives (8). From (20), we can replace ϕ with tanh in (13) and also use the difference of (22) and (23) to reexpress $\xi - \xi_1$, in order to obtain (9).

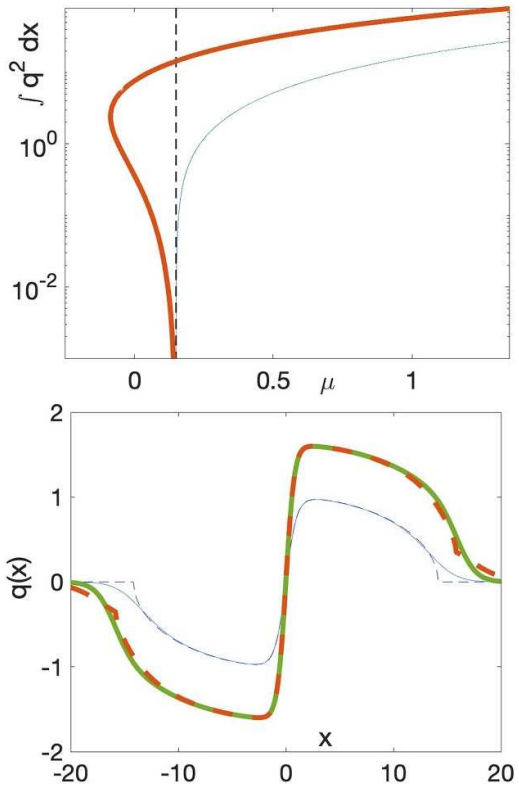

Figure 3. (Top panel) Similar to figure 1, but now for the prototypical dark soliton structure. Once again, the trap strength is $\Omega = 0.1$, hence the linear limit of the (harmonic oscillator) first excited state lies at $\mu = 3\Omega/2 = 0.15$. The thin blue line of the GPE is compared to the red thick line of the droplet case dark soliton branch continuation. (Bottom panel) Comparison of the respective dark solitons. The thin blue lines reflect the GPE result: here, the solid line shows the numerical dark soliton, while the dashed one represents the TF approximation multiplied by the tanh soliton profile). The respective droplet model states, also for $\mu = 1$ (as in the GPE) are shown by thick lines, with the analytical (dashed line) state arising from the multiplication of equation (11) by the analytical solitary wave of [26].

4. An extension: dark solitons

Having constructed a uniform approximation to the ground state of the quantum droplet model in the large μ limit, we now turn to an interesting extension of the relevant waveform. In particular, it is well-known that for the standard GPE model, the excited states in the form of dark solitons can be well-approximated in the large density (large chemical potential) limit by the ground TF state multiplied by the dark soliton of the homogeneous equation [35]. A relevant example for chemical potential $\mu = 1$ and $\Omega = 0.1$ is shown in the bottom panel of figure 3 (see, in particular, the thin lines therein). The central portion of the corresponding one-soliton stationary, anti-symmetric excited state wavefunction (the so-called black soliton [36]) is very well approximated by $\tanh(x)$, while the remaining waveform, aside from the boundary layer discussed in section I, is well approximated by the TF profile.

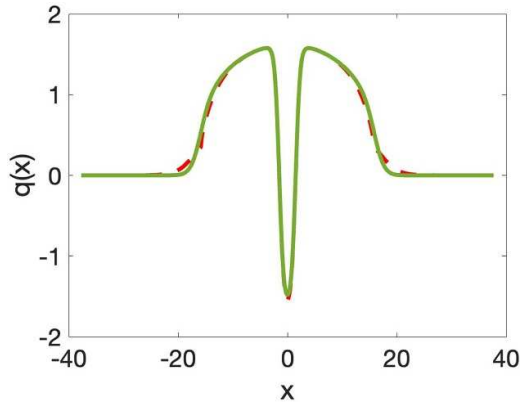

Figure 4. In this figure we have computed numerically the 2nd excited state (bearing 2 dark solitons) and have illustrated it in the same way as before for $\mu = 1$. Here also, the theoretical waveform is given by a dashed (red) line that can barely be distinguished from the numerically computed 2nd excited state solution with unit chemical potential shown in green (solid) line. The theoretical prediction is obtained the multiplication of equation (11) by two analytical solitary waves whose form is provided in [26] (and which are centered roughly at ± 1.5).

It is then natural to expect that a similar strategy can be used to *analytically* approximate, in a uniform way, black solitons in the quantum droplet model, which have been the subject of intense recent research efforts [24, 26, 27]. In particular, we leverage the analytical approximation of equation (11) for the ground state and multiply the relevant spatial profile by the exact analytical dark soliton of the homogeneous quantum droplet setting, as derived in [26]. Indeed, we use a similar notation as that work labeling $q_+ = (\delta + \sqrt{\delta^2 + 4\mu})/2$ and expressing the black soliton as:

$$u_{dark}(x) = q_+ + \frac{-\mathcal{B}(\mu) + \sqrt{\mathcal{B}^2(\mu) - 4\mathcal{A}(\mu)\mathcal{C}(\mu)}}{2\mathcal{A}(\mu)}, \tag{24}$$

in which expression the symbols $\mathcal{A}$, $\mathcal{B}$ and $\mathcal{C}$ are given by: $\mathcal{A}(\mu) = B^2 - 4A\tanh^2(\sqrt{A}(x))$, $\mathcal{B}(\mu) = 4AB\,\mathrm{sech}^2(\sqrt{A}(x))$, and $\mathcal{C}(\mu) = 4A^2\,\mathrm{sech}^2(\sqrt{A}(x))$, with $A = 4\mu + (1 + \sqrt{1+4\mu})$ and $B = 2(\frac{1}{3} + \sqrt{1+4\mu})$. It is important to recall that the expression of equation (24) can be used only for x such that $u_{\rm dark} > 0$, while the profile is supposed to be anti-symmetric around the point of zero crossing. Notice that also the point of zero crossing in the homogeneous model can be shifted at will due to the translational invariance of the underlying setting. By centering the relevant dark soliton around the center of the trap, as is expected for the stationary trapped black soliton state, and multiplying it by equation (11), we observe in the bottom panel of figure 3 that we get a very accurate approximation (thick dashed line) to the full numerical result (thick solid line). This happens for large chemical potentials ($\mu \gg \Omega$) for the branch of dark solitary wave solutions that is shown in the top panel of the figure, once again compared between the GPE and the EGPE models, in order to observe the impact of the attractive (beyond-mean-field) nonlinear term in the latter. This, in turn, can be the basis for analyses similar to those of [35] that may enable the systematic characterization of excited (multiple dark solitary wave) states stability and dynamics. Indeed, in principle, the usefulness of our analytical findings has a clear bearing to arbitrary excited states of the system, as is illustrated in the prototypical example of figure 4. Here, using a pair of dark solitons, again analytically

leveraged from [26] centered at (approximately) $x_0 = \pm 1.5$, we can very accurately describe *analytically* a 2nd excited state, bearing two dark solitons in the large chemical potential limit. Indeed, we have verified that this can also be done for the 3rd excited state, bearing 3 dark solitons etc. This paves the way for understanding *arbitrary* excited states of the system in 1d and, naturally, one can envision (upon availability of the respective ground state) similar generalizations involving, e.g. vortical states in higher dimensions, including in the experimental setting of [6].

5. Conclusions and future challenges

In this work we have analyzed the ground state of the EGPE in the presence of a parabolic confinement in the regime of the so-called TF limit, i.e. for the case of large densities/chemical potentials. We combined a separation of the spatial domain into different regions (the central region, the rapid transition—interface—region and the asymptotic state region) along with an analysis of each one through suitable rescalings and asymptotic methods in order to extract a uniformly valid asymptotic formula that we tested in direct numerical computations via fixed point iteration methods to provide an increasingly accurate description of the quantum droplet in the large density regime.

Naturally, this development paves the way for a number of possible considerations for the future. On the one hand, this naturally poses the question of whether approximate excitation frequencies for the quantum droplet can be extracted in this limit, by analogy of what has been done for the case of the standard GPE; see, e.g. the discussion of [37]. On the other hand, the availability of such an analytical 'ansatz' for a TF solution may offer the backdrop for the consideration of the asymptotic form of higher excited states, such as multiple dark solitons, in analogy with earlier works that were able to derive effective particle equations for such coherent structures [35]. Another meaningful extension of the present considerations is to the full two-component model for the two ^{39}K hyperfine states (such as $|1,-1\rangle$ and $|1,0\rangle$) for arbitrary density and scattering length variations; see, e.g. [17] for a relevant generalized model. At the same time, such analysis can provide a starting point for the consideration of higher dimensional analogues of the model and the asymptotic analysis of both droplet, but also importantly vortical patterns therein [21, 25]. Indeed, recent studies [38, 39] have extensively explored associated vortex lattice states in the presence of rotation. Such studies are currently in progress and will be presented in future publications.

Data availability statement

All data that support the findings of this study are included within the article (and any supplementary files).

Acknowledgments

This material is based upon work supported by the U S National Science Foundation under the Awards PHY-2110030 and DMS-2204702 (PGK), and DMS-2055072 (JH). PGK gratefully acknowledges numerous insightful discussions with S I Mistakidis, G C Katsimiga, R Carretero-González, S Chandramouli B A Malomed, G N Koutsokostas and D J Frantzeskakis on the subject of quantum droplets.

ORCID iDs

J Holmer https://orcid.org/0000-0003-3644-5549
K Z Zhang https://orcid.org/0000-0002-8515-6041
P G Kevrekidis https://orcid.org/0000-0002-7714-3689

References

[1] Petrov D S 2015 *Phys. Rev. Lett.* **115** 155302
[2] Khan A and Debnath A 2022 *Front. Phys.* **10** 887338
[3] Schmitt M, Wenzel M, Böttcher F, Ferrier-Barbut I and Pfau T 2016 *Nature* **539** 259
[4] Chomaz L, Ferrier-Barbut I, Ferlaino F, Laburthe-Tolra B, Lev B L and Pfau T 2022 *Rep. Progr. Phys.* **86** 026401
[5] Cabrera C R, Tanzi L, Sanz J, Naylor B, Thomas P, Cheiney P and Tarruell L 2018 *Science* **359** 301
[6] Cheiney P, Cabrera C R, Sanz J, Naylor B, Tanzi L and Tarruell L 2018 *Phys. Rev. Lett.* **120** 135301
[7] D'Errico C, Burchianti A, Prevedelli M, Salasnich L, Ancilotto F, Modugno M, Minardi F and Fort C 2019 *Phys. Rev. Res.* **1** 033155
[8] Semeghini G, Ferioli G, Masi L, Mazzinghi C, Wolswijk L, Minardi F, Modugno M, Modugno G, Inguscio M and Fattori M 2018 *Phys. Rev. Lett.* **120** 235301
[9] Lee T D, Huang K and Yang C N 1957 *Phys. Rev.* **106** 1135
[10] Petrov D S and Astrakharchik G E 2016 *Phys. Rev. Lett.* **117** 100401
[11] Ferioli G, Semeghini G, Terradas-Briansó S, Masi L, Fattori M and Modugno M 2020 *Phys. Rev. Res.* **2** 013269
[12] Fort C and Modugno M 2021 *Appl. Sci.* **11** 866
[13] Mistakidis S, Volosniev A, Barfknecht R, Fogarty T, Busch T, Foerster A, Schmelcher P and Zinner N 2023 *Phys. Rep.* **1042** 1
[14] Mithun T, Maluckov A, Kasamatsu K, Malomed B A and Khare A 2020 *Symmetry* **12** 174
[15] Mithun T, Mistakidis S I, Schmelcher P and Kevrekidis P G 2021 *Phys. Rev.* A **104** 033316
[16] Otajonov S R, Tsoy E N and Abdullaev F K 2022 *Phys. Rev.* A **106** 033309
[17] Tylutki M, Astrakharchik G E, Malomed B A and Petrov D S 2020 *Phys. Rev.* A **101** 051601(R)
[18] Englezos I A, Mistakidis S I and Schmelcher P 2023 *Phys. Rev.* A **107** 023320
[19] Stürmer P, Tengstrand M N, Sachdeva R and Reimann S M 2021 *Phys. Rev.* A **103** 053302
[20] Cappellaro A, Macrì T and Salasnich L 2018 *Phys. Rev.* A **97** 053623
[21] Li Y, Chen Z, Luo Z, Huang C, Tan H, Pang W and Malomed B A 2018 *Phys. Rev.* A **98** 063602
[22] Gangwar S, Ravisankar R, Muruganandam P and Mishra P K 2022 *Phys. Rev.* A **106** 063315
[23] Kartashov Y V, Lashkin V M, Modugno M and Torner L 2022 *New J. Phys.* **24** 073012
[24] Edmonds M 2023 *Phys. Rev. Res.* **5** 023175
[25] Saqlain S, Mithun T, Carretero-González R and Kevrekidis P G 2023 *Phys. Rev.* A **107** 033310
[26] Katsimiga G C, Mistakidis S I, Koutsokostas G N, Frantzeskakis D J, Carretero-González R and Kevrekidis P G 2023 *Phys. Rev.* A **107** 063308
[27] Katsimiga G C, Mistakidis S I, Malomed B A, Frantzeskakis D J, Carretero-Gonzalez R and Kevrekidis P G 2023 *Condens. Matter.* **8** 67
[28] Luo Z, Pang W, Liu B, Li Y and Malomed B A 2021 *Front. Phys.* **16** 32201
[29] Pethick C J and Smith H 2008 *Bose-EInstein Condensation in Dilute Gases* (Cambridge university press)
[30] Stringari S and Pitaevskii L 2003 *Bose-EInstein Condensation* (Oxford University Press)
[31] Gallo C and Pelinovsky D E 2011 *Asymptot. Anal.* **73** 53
[32] Karali G and Sourdis C 2015 *Arch. Ration. Mech. Anal.* **217** 439
[33] Salasnich L, Parola A and Reatto L 2002 *Phys. Rev.* A **65** 043614
[34] Mateo A M n and Delgado V 2008 *Phys. Rev.* A **77** 013617
[35] Coles M P, Pelinovsky D E and Kevrekidis P G 2010 *Nonlinearity* **23** 1753
[36] Frantzeskakis D J 2010 *J. Phys. A: Math. Theor.* **43** 213001
[37] Kevrekidis P G and Pelinovsky D E 2010 *Phys. Rev.* A **81** 023627
[38] Nikolaou S, Kavoulakis G M and Ögren M 2023 *Phys. Rev.* A **108** 053309
[39] Yoğurt T A, Tanyeri U, Keleş A and Oktel M O 2023 *Phys. Rev.* A **108** 033315